Triggered incommensurate transition in $PbHfO_3$

Roman G. Burkovsky,[1,*] Iurii Bronwald,[2,1] Daria Andronikova,[2,1] Georgiy Lityagin,[1] Julita Piecha,[3] Sofia-Michaela Souliou,[4,5] Andrzej Majchrowski,[6] Alexey Filimonov,[1] Andrey Rudskoy,[1] Krystian Roleder,[3] Alexei Bosak,[4] and Alexander Tagantsev[2,7]

[1]*Peter the Great Saint-Petersburg Polytechnic University, 29 Politekhnicheskaya, 195251 St. Petersburg, Russia*

[2]*Ioffe Institute, 26 Politekhnicheskaya, 194021 St. Petersburg, Russia*

[3]*Institute of Physics, University of Silesia, ulica 75 Puuku Piechoty 1, 41-500 Chorzów, Poland*

[4]*European Synchrotron Radiation Facility, BP 220, F-38043 Grenoble Cedex, France*

[5]*Karlsruher Institut für Technologie, Institut für Festkörperphysik, 76021 Karlsruhe, Germany*

[6]*Institute of Applied Physics, Military University of Technology, ulica Gen. W. Urbanowicza 2, 00-908 Warszawa, Poland*

[7]*Swiss Federal Institute of Technology (EPFL), School of Engineering, Institute of Materials Science, CH-1015 Lausanne, Switzerland*

(Received 4 March 2019; revised manuscript received 5 July 2019; published 29 July 2019)

We report a type of structural phase transitions in dielectric materials: the triggered incommensurate (IC) transition. We demonstrate evidence for such a transition in the perovskite antiferroelectric $PbHfO_3$ by means of single-crystal x-ray diffraction, diffuse, and inelastic-scattering experiments, which we interpret using the Landau theory of phase transitions. This transition is not driven by an IC soft mode, as is the case for the majority of IC dielectrics, but by the soft mode associated with a different, coexisting order parameter related to antiferrodistortive (AFD) tilts of the oxygen octahedra. When cooling from the high-temperature cubic phase these two order parameters are established simultaneously and discontinuously at $T_{IC} \approx 468$ K. Two lattice instabilities are present in the cubic phase: AFD instability with critical temperature $T_0 \approx 441$ K and ferroelectric instability with $T_0 \approx 408$ K. The IC instability is absent. The analysis of the transition mechanism within the Landau theory of coupled order parameters indicates that the transition is of triggered character, conditioned upon the attractive biquadratic coupling between the IC modulation and the AFD octahedral tilts, and is driven by the AFD soft mode.

DOI: 10.1103/PhysRevB.100.014107

I. INTRODUCTION

Incommensurate (IC) phases are a fascinating subject in solid-state science. They are characterized by the presence of an additional periodicity in the crystal, which coexists with the basic, standard crystalline periodicity, and evolves independently of it on changing external conditions, such as pressure or temperature [1,2]. Phase transitions leading to incommensuration are so unusual and counterintuitive that one of their pioneering theorists, Lifshitz, initially discarded the very possibility of their existence in the form, by which we mainly know them today [2].

The mechanisms driving the formation of IC structures can be very different for different kinds of IC systems and normally present substantial scientific challenges [3]. Especially difficult appear the cases of IC dielectrics, in which the atomic-level mechanisms of formation are highly complex and often controversial [2,4–6]. However, on the level of phenomenological description, which is an upper layer of the theory, the IC transitions in dielectrics are known to follow the universal route [2]. This route implies that the high-symmetry (usually high-temperature) phase is characterized by an IC soft mode. This mode can be of phonon character in displacive systems, such as K_2SeO_4 [7], or of pseudospin character in order-disorder systems [8], such as $NaNO_2$ [9]. It is associated with a maximum of generalized susceptibility (minimum of generalized stiffness [10]) at finite wave vector. The formation of IC modulation is preceded by the divergence of susceptibility at its maximum (decrease of stiffness down to zero) at the transition temperature. Apart from the very few exceptions [11], the IC transitions take place in a highly continuous way, being the transitions of the second order.

Here we report on a conceptually different type of IC transition in dielectrics: the triggered IC transition. This transition becomes possible when, apart from the IC displacement wave, there is another (second) order parameter present. The two order parameters appear simultaneously at the transition temperature in a highly discontinuous manner (first-order phase transition). In contrast to the standard route of IC transitions, there is no IC soft mode in the high-symmetry phase, but there is a soft mode associated with the second order parameter. The softening of this mode drives the composite transition, in which the IC modulations appear as a result.

We demonstrate evidence for such a transition in perovskite antiferroelectric $PbHfO_3$ [12] using complementary x-ray diffraction, diffuse, and inelastic-scattering experiments. $PbHfO_3$ has three phases at ambient pressure: low-temperature antiferroelectric (AFE) phase $A1$, defined by antipolar Pb^{2+} cation shifts and antiferrodistortive (AFD) oxygen octahedral tilts, the intermediate AFE phase $A2$ [13–18] (433 K $< T <$ 478 K [17]), which is similar to $A1$,

*roman.burkovsky@gmail.com

but with antipolar displacements organized in a wave of larger period [19], and the high-temperature cubic phase. We show that the $A2$ phase is an IC phase, which forms as the result of a triggered IC transition driven by the AFD soft mode. The finding bridges the research areas of triggered structural transformations [20–24], IC phase transitions in dielectrics [2], and antiferroelectricity in functional perovskites [25].

The paper is organized as follows. First, using single-crystal x-ray diffraction, we demonstrate that the long-period modulation in the $A2$ phase is an IC modulation, as evidenced by highly continuous evolution of the modulation wave vector with temperature. Second, on the basis of an exhaustive investigation of possible lattice instabilities in the cubic phase using diffuse and inelastic x-ray scattering (IXS), we establish the absence of an IC soft mode, but the presence of FE and AFD soft modes. Finally, invoking the analysis of the present lattice instabilities within Landau theory, we outline the transition scenario, discuss and conclude the paper.

II. METHODS

A. Single-crystal sample preparation

$PbHfO_3$ single crystals were synthesized by means of spontaneous crystallization from the high-temperature solution in a Pb_3O_4-B_2O_3 solvent. The composition of the melt used in our experiments was as follows: 2.4 mol % of $PbHfO_3$, 77 mol % of PbO (re-counted to Pb_3O_4) and 20.6 mol % of B_2O_3. The Pb_3O_4 was used instead of PbO to avoid coloration of the as-grown crystals caused by oxygen deficiency. The crystallization was carried out in a platinum crucible covered with a platinum lid under conditions of a low-temperature gradient. After soaking at 1473 K for 24 h the melt was cooled down to 1200 K at a rate of 3.5 K/h and after decantation the furnace was cooled to room temperature at a rate of 10 K/h. As-grown $PbHfO_3$ single crystals were etched in diluted acetic acid to remove residues of the solidified flux. For use in diffraction, diffuse scattering, and IXS experiments we have prepared samples in the form of needles with 40×40 micron cross section.

B. Diffraction and IXS characterization

We have used high-precision single-crystal x-ray diffraction to study temperature dependence of modulation wave vector, energy-integrated diffuse scattering—to characterize static susceptibility with respect to transverse modulations in cubic phase, and energy-resolved IXS experiment to study oxygen-related modes that are inaccessible in diffuse scattering (DS) experiment due to comparably weak scattering by oxygen ions.

The diffraction and IXS experiments were carried out at the two experimental stations of ID28 beamline of the European Synchrotron Radiation Facility (ESRF) [26]. The diffraction side station was operating at the wavelength 0.6583 Å. The diffraction images were collected using Dectris Pilatus 1M detector (172×172 micron pixel size) positioned at the distance of 32.6 cm from the sample position. The data were collected with angular step of 0.1° rotation per 0.1 s of exposure. The same setup has been used for diffraction and diffuse scattering measurements. The data collection has been performed in the energy-integrating mode. The DS analysis has been performed near the reciprocal-lattice node (−1 2 0), which has very weak structure factor for Bragg scattering and, consequently, negligible contribution from acoustic phonons to the DS signal. The reciprocal space maps of scattering intensity were constructed using CRYSALIS PRO software and custom-built MATLAB codes. Additional diffraction measurements in the IC phase have been carried out using a SuperNova (Oxford Diffraction) laboratory diffractometer in order to reliably reconstruct the modulation wave-vector temperature dependence in the whole IC phase stability range (see Appendix A for details).

The IXS station was operating Si (9 9 9) backscattering monochromator reflection which corresponds to the wavelength 0.6968 Å and energy resolution about 3 meV (full width at half maximum). For each IXS scan the spectra at nine different positions in the reciprocal space were simultaneously recorded due to the use of an array of analyzer-detector pairs. Analysis of IXS spectra has been performed using a standard model composed of a damped harmonic oscillator response function [27], to account for phonon peaks, and a Lorentzian-shaped peak, to account for the central component in the spectra. The sum of these components was convoluted with the standard pseudo-Voigt resolution function.

Temperature control during diffraction and IXS measurements was achieved using heat blowers.

III. RESULTS

A. Proof of incommensuration

Diffraction images show the superstructure reflections corresponding to two order parameters: transverse modulations and AFD tilts. Figure 1(a) shows the intensity distribution in two reciprocal space planes: $(H, K, 0)$ and $(H, K, -1.5)$ at $T = 453$ K ($A2$ phase). The former plane shows a series of satellite reflections with wave vectors of the form $\vec{Q} = (H + n\xi_0, K + n\xi_0, L)$, where H, K, L, and n are integers and $\xi_0 \sim 0.15$ is the component of the modulation wave vector $\vec{q}_0 = (\xi_0, \xi_0, 0)$. The positions of these satellites, as well as their conditions of observability in different Brillouin zones, indicate their origin as transverse displacive modulation analogous to the one of the low-temperature $A1$ AFE phase, but with different modulation wave vector. The $(H, K, -1.5)$ plane contains the reflections at the R points of the Brillouin zone of the form $\vec{Q} = (H + \frac{1}{2}, K + \frac{1}{2}, L + \frac{1}{2})$ and their satellites at $\vec{Q} = (H + \frac{1}{2} + n\xi_0, K + \frac{1}{2} + n\xi_0, L + \frac{1}{2})$. The R-point reflections indicate the presence of antiphase oxygen octahedral tilts, analogous to the ones characteristic to the $A1$ phase.

In contrast to the previous results [19], which imply a long-period commensurate structure, our data clearly indicate incommensuration. We have performed the diffraction measurements on a fine temperature grid ($\Delta T = 1$ K, from $T = 475$ K down to $T = 453$ K) and traced the behavior of the highest order satellites, which are the most sensitive to the changes in the modulation wave vector. Figure 1(b) shows the temperature dependence of the intensity distribution along the [1 1 0] direction. An interesting observation is that the satellites with order pairs such as (2 and −5) or (3 and −4)

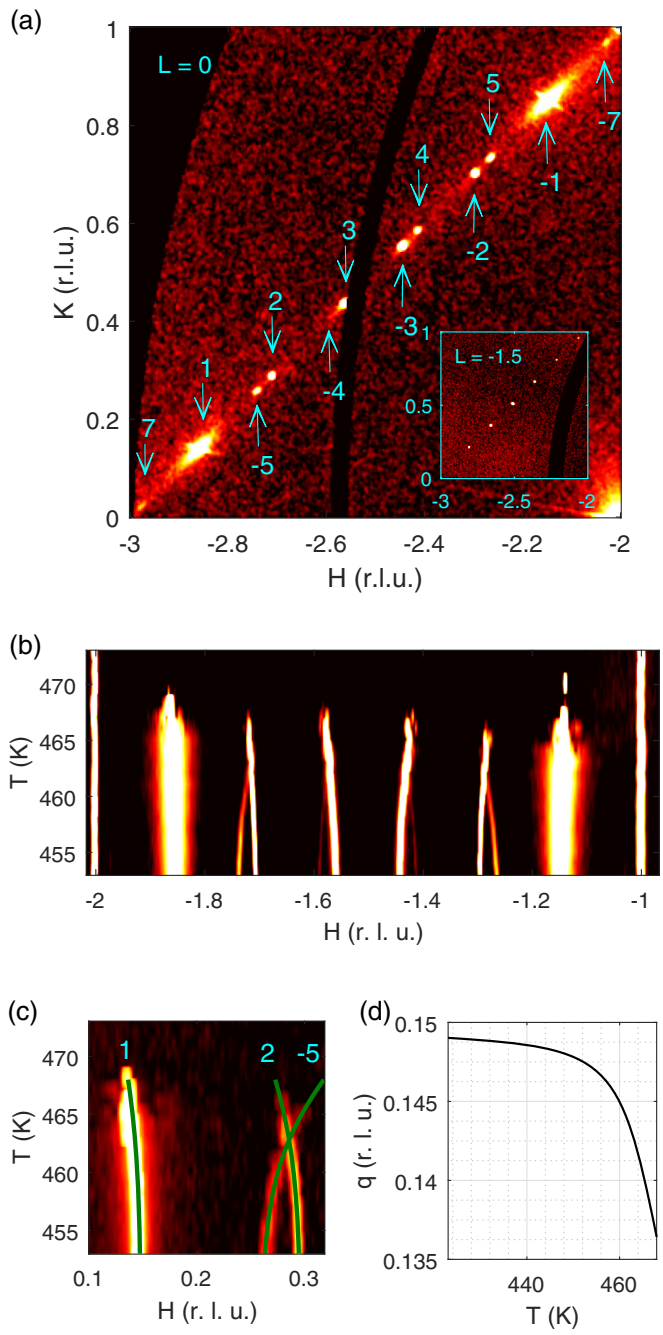

FIG. 1. Single-crystal x-ray-diffraction results. (a) Reciprocal space map of $PbHfO_3$ in $(H, K, 0)$ plane in pseudocubic coordinates at $T = 453$ K. Arrows denote satellite reflections of orders up to 7. The inset shows the map for $(H, K, -1.5)$ plane containing the R-point reflection and its satellite reflections. The intensity scale is logarithmic. (b) Temperature dependence of the diffraction pattern along the series of superstructure reflections located between $(-2\ 1\ 0)$ and $(-1\ 2\ 0)$ pseudocubic reflections. (c) The same, but with the emphasis on the 2nd- and -5th-order superstructure reflections (the -6th-order satellite is not visible due to the overlapping with the strong signal from the 1st-order satellite). Solid lines denote the positions of satellites of different orders corresponding to the single continuous approximation to $\xi_0(T)$. (d) Temperature dependence of the component ξ_0 of the modulation wave vector $\vec{q}_0 = (\xi_0, \xi_0, 0)$.

are merging close to the transition temperature between the $A2$ and cubic phases. The enlarged area of the map [Fig. 1(c)] shows that this merging takes place solely at a particular temperature (as opposed to an extended temperature range), where the trajectories of the relevant satellites intersect with each other. At this temperature (≈463 K), the modulation wave-vector component ξ_0 has a commensurate value $\frac{1}{7}$. Such low-order rational values are known to be potential hosts for temporary commensuration in "incomplete devil's staircases" [2,28], but our data show that this is not the case for $PbHfO_3$. The overall continuity of $\xi_0(T)$ is very high. Figures 1(c) and 1(d) show this dependence by solid lines. It increases monotonically on cooling, and approaches saturation at about 0.149 before experiencing a discontinuous increase to $\xi_0 = 1/4$ (not shown) on the lock-in transition to the commensurate AFE phase. Refer to Appendix A for more details on determining $\xi_0(T)$ dependence.

B. Two lattice instabilities

How does it occur that the two order parameters appear jointly on cooling? AFD transitions in perovskites are typically due to the AFD lattice instability associated with AFD soft mode [10]. IC transitions in dielectrics are typically driven by the IC soft mode condensation [2]. It naturally follows that $PbHfO_3$ has to possess these two soft modes in the cubic phase. We show that this is not the case: there are only FE and AFD instabilities instead, the latter being characterized by the highest critical temperature.

Generalized static susceptibility associated with the IC order parameter is linked to diffuse scattering intensity as $I(\vec{Q}, T) \propto T\chi(\vec{q}, T)$ [10], where the wave vector $\vec{q}$ is the difference between wave vector transfer $\vec{Q}$ and a reciprocal-lattice vector. Figure 2(a) shows the DS intensity distribution in the $(H, K, 0)$ reciprocal space plane for $T = 473$ K, which is just above the transition temperature of 468 K. The largest intensity values reside along the lines of the form $\vec{q} = (\xi, \xi, 0)$, which include the wave vector $\vec{q}_0$ of the modulation in the IC phase.

Interestingly, the DS intensity distribution does not have a maximum or any specific feature at the wave vector $\vec{q}_0$, at which the IC superstructure reflection appears on cooling. This contrasts with the picture recently reported in $PbZrO_3$ under pressure [29], and with diffuse scattering studies of classical IC dielectrics [9,30,31], where the finite wave-vector critical scattering maximum has been observed.

To guarantee the absence of any critical behavior associated specifically with $\vec{q}_0$, we have performed the joint numerical analysis of DS distributions corresponding to different temperatures using the simplest possible Taylor expansion of generalized static stiffness. Along the direction of interest, $\vec{q} = (\xi, \xi, 0)$, this expansion should assume the form [2]

$$\chi^{-1}(\xi, T) = A(T - T_0) + D(\xi - \xi_m)^2, \qquad (1)$$

where A and D are constants and ξ_m is the wave vector of stiffness minimum. In the case of the IC soft mode present, this expansion would be valid in a relatively narrow wave-vector range around $\xi_m = \xi_0$. Obviously, this is not the case, because the susceptibility has a large nonzero slope at ξ_0 [Fig. 2(b)].

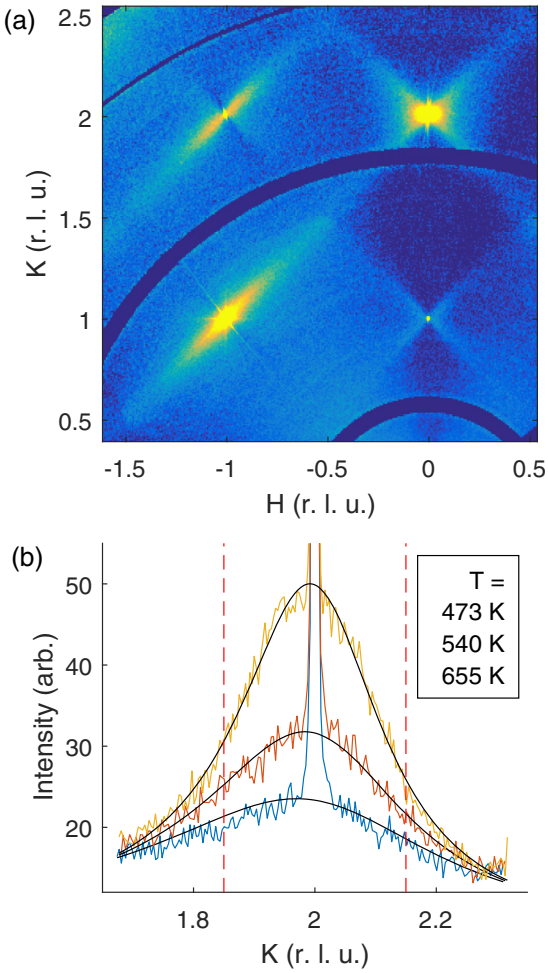

FIG. 2. Diffuse scattering distribution in the cubic phase and its evolution with changing temperature. Panel (a) shows the two-dimensional distribution in the $(H, K, 0)$ plane, panel (b) shows one-dimensional profiles along [1 1 0] direction together with fit results as described in the text. The DS intensity increases on cooling towards the transition temperature of about 468 K. Vertical dashed lines show the positions of the first-order IC satellites in the IC phase. In the cubic phase, the DS maxima would be expected at these positions in the case of the IC soft mode being present.

Vertical dashed lines show the positions of expected maxima. On the other hand, the experimental DS distributions are consistent with Eq. (1) for $\xi_m = 0$, implying the presence of a ferroelectric soft mode. The corresponding susceptibility distribution takes the form

$$\chi(\vec{q}, T) = \frac{1}{D}\frac{1}{\xi^2 + (A/D)(T - T_0)}, \tag{2}$$

which enters the formula for DS intensity as [10]

$$I(\vec{Q}, T) = T|F(\vec{Q})|^2\chi(\vec{q}, T) + I_{\text{Background}}, \tag{3}$$

where $\vec{Q}$ is the scattering vector and $F(\vec{Q})$ is the structure factor [32]. Notably, the DS profiles have Lorentzian shape and do not tend to diverge on approaching the zone center. This indicates a negligible contribution from scattering at acoustic phonons to the DS signal, compared to the scattering at the fluctuations of the order parameter.

The above equations (2) and (3) describe $I(\vec{Q}, T)$ consistently in a broad wave-vector range including ξ_0. Furthermore, the critical temperature $T_0 = 408$ K is quite consistent with the ferroelectric critical temperature obtained by dielectric measurements [33]. Considered together, these facts indicate that the moderate temperature dependence of DS at $\xi = \xi_0$ is conditioned upon the softening of ferroelectric soft mode, and not an IC soft mode. The IC soft mode is absent in the cubic phase.

Albeit there is no IC soft mode, the dispersion of ferroelectric soft mode in $PbHfO_3$ is more favoring the formation of IC modulations than in other ferroelectrics. Indeed, the D coefficient in $PbHfO_3$ is several times smaller than in normal ferroelectric $PbZr_{0.6}Ti_{0.4}O_3$. Andronikova *et al.* have determined the A/D ratio for that crystal [34], which turns out to be about 4.5 times smaller than we have found in the present study for $PbHfO_3$ ($A/D = 3.2 \times 10^{-4}$(r.l.u.)^2/K). Provided that the A parameters for $PbHfO_3$ and $PbZr_{0.6}Ti_{0.4}O_3$ are similar [35], the difference in A/D is mainly due to the difference in D coefficients. Therefore, in $PbHfO_3$ the D coefficient is several times smaller. As long as this coefficient controls the energy cost of creating polarization inhomogeneities [36], these inhomogeneities are created more easily in $PbHfO_3$ than in ferroelectrics. The specifics will be useful later in the discussion of the transition scenario.

C. AFD instability

When there is no IC soft mode, what is the driver for the IC transition? We show that the AFD instability is characterized by the highest critical temperature and the corresponding soft mode creates the necessary condition for the incommensuration to appear.

AFD tilts correspond to the R point of the pseudocubic Brillouin zone and are described by the Γ_{25} irreducible representation (IR) in the notation of Cowley [37]. Characteristic IXS spectra obtained by us at different temperatures and at different R points are shown by circles in Figs. 3(a)–3(c). The spectra comprise two relatively broad and temperature-independent sideband peaks and a highly temperature-dependent central peak located at zero energy transfer. The energy width of the central peak profile is determined largely by the width of the resolution function; the peak appears resolution limited. In the wave-vector space the central peak is also relatively narrow, as detailed in Appendix B. The sideband phonons are characterized by energy $\hbar\omega = 7.3 \pm 0.4$ meV and damping constant $\Gamma = 5.8 \pm 1.1$ meV and are temperature independent within the accuracy of parameter determination. These properties of sideband peaks are consistent with the ones obtained in previous study [38], which, however, did not allow identifying the relevant lattice modes and tracing the central peak temperature dependence, which is proven essential by the present results.

First, we identify the lattice modes responsible for sideband and central peak components of the spectra. The primary candidate is the oxygen tilt (AFD) mode, which corresponds to the Γ_{25} IR [37]. Indeed, this mode has been found the most unstable in first-principles study of similar crystal $PbZrO_3$ [39]. To check whether the observed sideband and central peaks correspond to Γ_{25} representation, we have performed

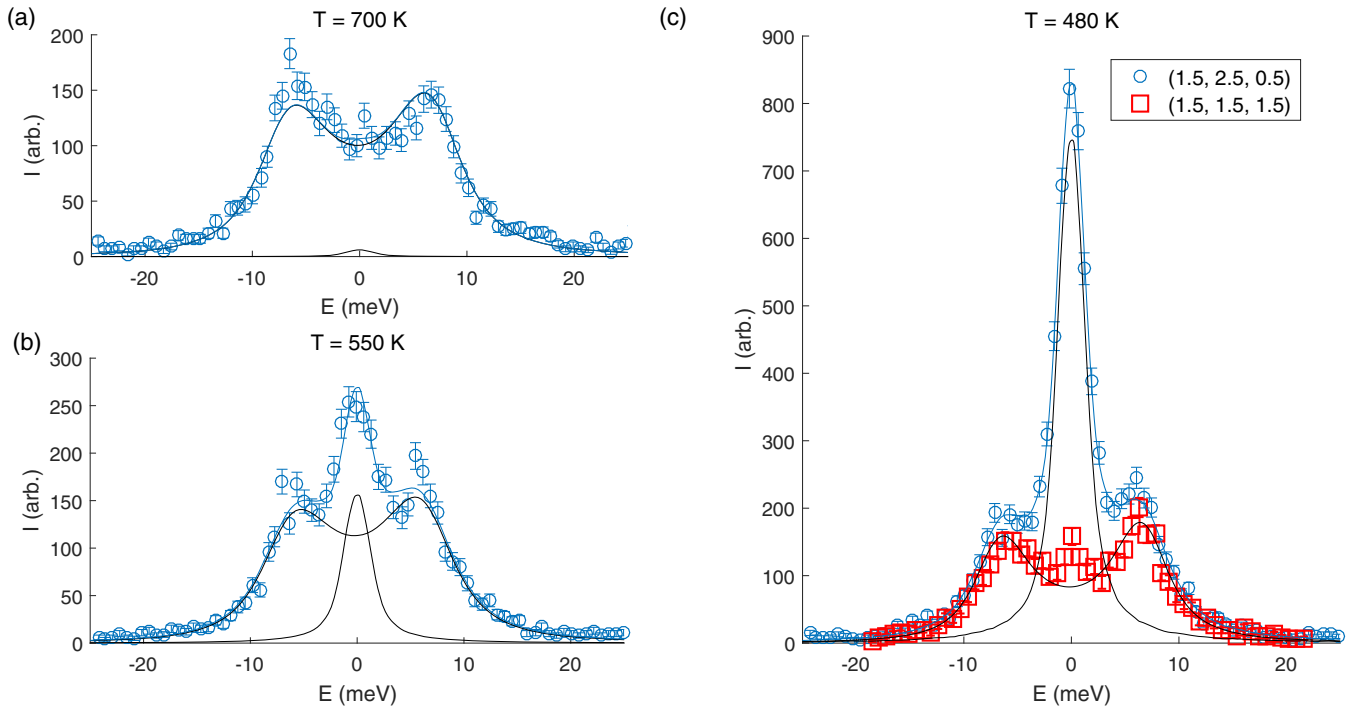

FIG. 3. Inelastic x-ray scattering results at the R points of the Brillouin zone. Panels (a)–(c) show evolution of the IXS spectrum with temperature at the R point (1.5, 2.5, 0.5) by circles, fit results by solid lines. Panel (c) shows, in addition, the spectrum at the R point (1.5, 1.5, 1.5) by squares, in which the central peak is nearly absent.

the IXS measurements at two distinct R points, (1.5, 1.5, 1.5) and (1.5, 2.5, 0.5). These two R points differ in the possibility of observing the signal due to the oxygen octahedral tilts [40]. In the case when all three coordinates have the same absolute value, which is true for the point (1.5, 1.5, 1.5), the scattering due to tilt modes is forbidden due to zero structure factor. When the coordinates are different, as it is the case for the point (1.5, 2.5, 0.5), the structure factor for tilts is nonzero and one may register the relevant scattering signal. In the case when sideband and central peaks would correspond to the same Γ_{25} representation, both these spectral features should disappear from the spectrum on going from (1.5, 2.5, 0.5) to (1.5, 1.5, 1.5). Experimentally it is not the case, as is clear from Fig. 3(c). Only the central peak disappears, while sideband peaks remain the same. Therefore, the central peak corresponds to the oxygen octahedral tilts (Γ_{25} AFD mode), while the sideband peaks correspond to some other lattice mode. The obvious candidate for sideband peaks is the Γ_{15} mode, which has been also found unstable, alongside with the Γ_{25} mode, by first-principles study of Ghosez *et al.* [39]. The scattering at the Γ_{15} phonons is not systematically forbidden at any of the R points. Furthermore, since the motion in the Γ_{15} mode is expected to be dominated by Pb-ion displacements [39], the inelastic structure factor is expected to be similar in magnitude at different R points characterized by similar magnitudes of scattering vector $|\vec{Q}|$. This is in good agreement with nearly identical sideband peak intensities in (1.5, 1.5, 1.5) and (1.5, 2.5, 0.5) points. This leads to the conclusion that the central and sideband peaks in the spectra correspond to the Γ_{25} and Γ_{15} modes, respectively.

In principle, the sideband phonon peaks due to the Γ_{25} AFD mode should be also present in the spectra at (1.5, 2.5, 0.5). Experimentally, we do not distinguish them. A tentative explanation is that the Γ_{25} sideband peaks are much weaker than the Γ_{15} sideband peaks (the atomic scattering factor for oxygen is much smaller than the one for Pb), and become indistinguishable on top of the latter [41].

Strongly temperature dependent and narrow in energy, central peaks are known to manifest the softening of AFD modes in perovskites [10,42]. The dominating role of a very sharp central peak in the AFD critical dynamics is well known for AFD transition in $SrTiO_3$ [43–46]. In that crystal, on approaching the AFD transition, the soft-mode dynamics experiences a crossover from a classical behavior with soft phonon resonances following Cochran's law $\omega^2_{\mathrm{AFD}}(T) \propto (T - T_0)$ to the regime, where the temperature dependence of these resonances is largely saturated at a finite nonzero value and the critical slowing down of the soft mode becomes represented by the central peak rapidly increasing in intensity [44]. This picture is consistent with our observations in $PbHfO_3$. By analyzing the central peak integral intensity as a function of temperature we estimate the critical temperature associated with the AFD soft mode. Assuming that this intensity is representative to the AFD static susceptibility, we have fitted its temperature dependence by the standard relation [10] $I(T) \propto T\chi(T)$ with $\chi(T) = 1/(T - T_0)^{\gamma}$ and obtained critical temperature $T_0 = 441$ K and index $\gamma = 1.26$. The index value is only slightly above unity (which would indicate the standard Curie-Weiss behavior), and can be possibly consistent with nonclassical behavior anticipated for this type of order parameter [10].

AFD instability is clearly present in $PbHfO_3$. It is manifested by the AFD static susceptibility diverging at about $T_0^{\mathrm{AFD}} = 441$ K, which is only slightly below the actual

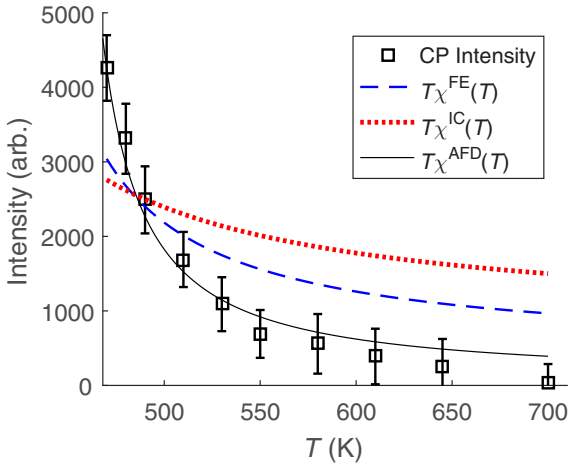

FIG. 4. Comparison of temperature dependencies of AFD, FE, and IC susceptibilities. The susceptibilities are plotted multiplied by temperature, in the form of $T\chi(T)$, to make them also comparable to the experimentally determined AFD central peak temperature dependence.

transition temperature of about 468 K and is substantially higher than the ferroelectric critical temperature of about 408 K. Comparison of temperature trends associated with different susceptibilities (AFD, FE, IC) is shown in Fig. 4. The dependence $T\chi^{FE}(T) = CT/(T - T_0^{FE})$ (dashed line), which is related to dielectric susceptibility, is substantially less sharp than the same relation for AFD susceptibility. The dependence $T\chi^{IC}(T)$ (dotted line), calculated using $\chi(T)$ of Eq. (2) with $\xi = \xi_0$, is very weakly temperature dependent (low critical temperature $T_0^{IC} = 340$ K), compared to AFD and dielectric susceptibilities. This weak temperature dependence is due to the finite wave-vector tail of the FE soft mode. The AFD critical temperature is the highest.

D. Transition scenario

How does the strong AFD instability result in the IC modulation despite the absence of finite wave-vector stiffness minimum? We show that the mechanism of their formation corresponds to a triggered transition, in which two order parameters appear simultaneously, similarly to the triggered ferroelectricity, which was initially identified by Holakovsky [20] and later discovered in $BiFeO_3$ using *ab initio* methods [23].

The simplest expansion of the thermodynamic potential that is allowed by cubic symmetry, involves the relevant order parameters and allows first-order transitions is [47]

$$G_\xi(A_\xi, \eta) = \frac{\alpha_\xi(T)}{2}|A_\xi|^2 + \frac{\beta_\xi}{4}|A_\xi|^4 + \frac{\alpha'(T)}{2}\eta^2 + \frac{\beta'}{4}\eta^4 + \frac{\gamma'}{6}\eta^6 + \frac{\delta_\xi}{2}|A_\xi|^2\eta^2. \quad (4)$$

Here, A_ξ is the amplitude of the complex wave $A_\xi \exp(i\vec{q}\vec{r})$, the real part of which is proportional to the components of ionic displacement vectors of the form $(u, -u, 0)$. Wavevector $\vec{q}$ is directed along [1 1 0]. η is the amplitude of the AFD order parameter. The coefficients $\alpha_\xi(T)$ and β_ξ describe the stiffness and anharmonism related to A_ξ, while the coefficients $\alpha'(T)$, β', and γ' correspond to η. The δ_ξ coefficient describes the wave-vector-dependent biquadratic interaction between the two order parameters.

Simultaneous formation of IC and AFD order parameters implies a minimum of G_ξ at nonzero A_ξ and η. This requires negative biquadratic coupling constant δ_ξ. Indeed, invoking the equation of state with respect to $|A_\xi|$,

$$0 = \partial G_\xi/\partial(|A_\xi|) = |A_\xi|(\alpha_\xi + \beta_\xi|A_\xi|^2 + \delta_\xi\eta^2), \quad (5)$$

and discarding the nonrelevant solution $A_\xi = 0$, we obtain

$$|A_\xi|^2 = \frac{-\delta_\xi\eta^2 - \alpha_\xi}{\beta_\xi}. \quad (6)$$

Since β_ξ is positive, the solution exists if $-\delta_\xi\eta^2 > \alpha_\xi$. As long as $\alpha_\xi > 0$ (from the experiment), this can be only possible when $\delta_\xi < 0$.

With negative δ_ξ, the condition $0 = \partial G_\xi/\partial(|A_\xi|)$ is fulfilled at nonzero A_ξ only for amplitudes of AFD tilts exceeding the limiting value $\eta^2 > -\alpha_\xi/\delta_\xi$. This shows that when IC stiffness is finite at the transition temperature, the whole transition can be only of the first order. The value of η at the transition temperature is obtained by analyzing Eq. (4), in which $|A_\xi|^2$ is replaced by the right-hand side of Eq. (6), resulting in the sixth-degree polynomial in η,

$$G'_\xi = -\frac{\alpha_\xi^2}{4\beta_\xi} + \frac{\alpha''(T)}{2}\eta^2 + \frac{\beta''}{4}\eta^4 + \frac{\gamma'}{6}\eta^6, \quad (7)$$

with renormalized coefficients $\alpha''(T) = \alpha'(T) - \alpha(T)\delta_\xi/\beta_\xi$ and $\beta'' = \beta' - \delta_\xi^2/\beta_\xi$. The value of η at the transition temperature is extracted from Eq. (7) using standard treatment of the first-order phase-transition theory, after which the value of $|A_\xi|$ is recovered using Eq. (6).

The visual comparison of $G_\xi(A_\xi, \eta)$ in the cases of negative and zero biquadratic coupling constant is shown in Fig. 5. For simplicity it is assumed that IC stiffness is temperature independent and the triggered transition is purely due to the AFD softening.

The IC nature of the transition requires, additionally, that the minimum in $G_\xi(A_\xi, \eta)$ corresponding to modulation wave vector $(\xi_0, \xi_0, 0)$, should be deeper than the similar minima corresponding to neighboring wave vectors with $\xi \neq \xi_0$. Therefore, the potential G, when considered as a function of three independent variables $(\xi, |A_\xi|, \eta)$, shall have an absolute minimum in these three variables, and this minimum shall correspond to $\xi = \xi_0$, $|A_\xi| \neq 0$, and $\eta \neq 0$ at the transition temperature.

The above mechanism of selecting modulation wave vector $[G(\xi, A_\xi, \eta) = \min]$ is different and more complex than the one in second-order IC transitions, where the wave vector is merely determined by the minimum in IC stiffness in the high-symmetry phase $[\alpha(\xi) = \min]$. The necessary condition for a minimum, $\partial G/\partial\xi = 0$ at $\xi = \xi_0$, cannot be fulfilled with only α_ξ being wave-vector dependent. Therefore, we have to assume wave-vector dependence for some of the anharmonic coefficients. It is known that AFD tilts tend to affect FE and AFE modes differently, suppressing ferroelectricity [48] and enhancing antiferroelectricity [49]. This implies that δ_ξ should be wave-vector dependent, being positive near the

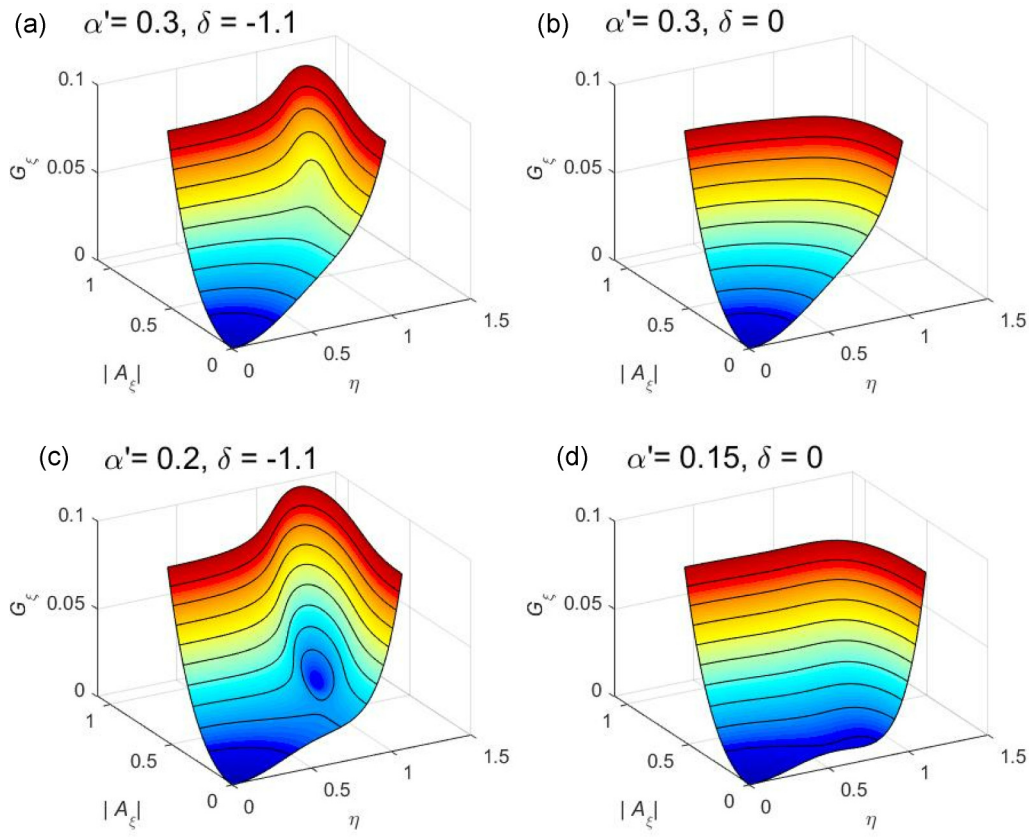

FIG. 5. Comparison of free-energy landscapes in the cases of negative and zero biquadratic coupling constant. In the case of negative constant (left side), decrease of AFD stiffness, $\alpha'(T)$, results in the formation of a minimum at nonzero IC and AFD order parameters, while for zero constant (right side), the minimum corresponds to purely AFD phase transition. The coefficients used in the plots are $\alpha_\xi = 0.5$, $\beta_\xi = 1.6$, $\beta' = -0.8$, $\gamma' = 1$.

Brillouin-zone center and negative near the zone boundary. Considering that only α_ξ and δ_ξ are wave-vector dependent, we can estimate the ξ dependence of δ_ξ on the basis of experimentally determined $\alpha_\xi = A(T - T_0) + D\xi^2$. Assuming that η attains its spontaneous nonzero value η_0, and substituting this value into $G(\xi, A_\xi, \eta)$, we find the latter function transformed to

$$G''_\xi(A_\xi) = \frac{\alpha^\eta_\xi(T)}{2}|A_\xi|^2 + \xi \text{ independent terms}, \qquad (8)$$

where $\alpha^\eta_\xi(T) = \alpha_\xi + \eta_0^2\delta_\xi$ is the renormalized IC stiffness. Requiring the renormalized stiffness to have a minimum that is touching the zero level at $\xi = \xi_0$ ($\alpha^\eta_\xi = 0$, $\partial\alpha^\eta_\xi/\partial\xi = 0$, $\partial^2\alpha^\eta_\xi/\partial\xi^2 > 0$), we obtain the following expectations on δ_ξ:

$$\delta(\xi_0) = -\left[A(T - T_0) + D\xi_0^2\right]/\eta_0^2, \qquad (9)$$

$$\frac{\partial\delta}{\partial\xi} = -2D\xi_0/\eta_0^2, \qquad (10)$$

$$\frac{\partial^2\delta}{\partial\xi^2} > -2D/\eta_0^2. \qquad (11)$$

Since $T - T_0$ is relatively small near the transition temperature, and D is also relatively small, we find these expectations not very demanding. δ_ξ has to be moderately negative at $\xi = \xi_0$ and its derivative has to be moderately negative. The curvature can be positive or negative, but in the latter case, its absolute value should not be too large. Importantly, δ_ξ is not required to have a minimum at or near ξ_0. These characteristics of δ_ξ are quite consistent with the ones envisaged from the atomistic considerations [48,49] and, therefore, indicate the fitness of the scenario.

The model predicts an increase of the modulation vector length on cooling. Equation (10) implies $\xi_0 = \text{Const} \times \eta_0^2$, from which it follows that an increase of the AFD order-parameter amplitude on cooling leads to the increase of ξ_0. This is in agreement with the experiment.

IV. DISCUSSION

The difference between triggered incommensuration in $PbHfO_3$ and classical Holakovsky triggering of ferroelectricity [20] is not only in the nature of order parameter, which is IC modulation and FE polarization, respectively, but also in the possibility of formally defining the primary order parameter [21]. In the Holakovsky scenario the only temperature-dependent susceptibility is AFD susceptibility, while in $PbHfO_3$ the IC susceptibility depends on temperature as well. However, the strong quantitative difference in critical temperatures together with the absence of susceptibility maximum at the IC wave vector allow identifying the AFD soft mode as the driver of the triggered transformation.

It is instructive to address the difference between transition scenarios in $PbHfO_3$ and $PbZrO_3$ crystals, which are similar from the crystallochemical point of view [50]. In

$PbZrO_3$, at ambient pressure, the transition goes directly to the commensurate AFE phase, which is determined by stronger influence of the terms *commensuralizing* the modulation, such as Umklapp interaction [47] and interaction with minor additional distortions [51,52]. The AFD susceptibility has been reported only weakly temperature dependent in $PbZrO_3$ [47,53]. Therefore, the simultaneous appearance of AFE and AFD modulations in that crystal can be attributed to the triggered transition driven primarily by the softening of IC stiffness in the presence of commensuralizing interactions. In $PbHfO_3$, in contrast, the dominating instability is the AFD instability, which enables the triggered formation of IC phase before the commensuralizing effects lead to the lock-in transition to the commensurate AFE phase. The suppression of the FE phase transition, in both cases, has to be understood as the result of repulsive biquadratic couplings to IC and/or AFD order parameters.

V. CONCLUSION

We have identified a triggered IC transition. In contrast to the classical route of IC soft-mode-driven transitions, a triggered IC transition occurs due to the presence of another structural instability associated with the soft mode. In $PbHfO_3$ the role of this instability is the well-known and widely studied AFD instability linked to antiphase oxygen octahedral tilts. Approaching the soft-mode-driven AFD transition on cooling results in the creation of a minimum in free-energy landscape at nonzero IC and AFD order parameters, which enables the combined IC + AFD phase transition instead of the sole AFD transition.

Interestingly, purely AFD phases have not yet been identified in lead-based antiferroelectrics, but our present results suggest that they could be eventually found at conditions inhibiting the antipolar cationic shifts.

Understanding the interplay between the cation ordering and oxygen octahedral tilts in AFE perovskites has been challenging, especially at high temperatures, where the *ab initio* based theory is yet only starting to be developed. Such a specific behavior as triggered incommensuration should provide a very useful benchmark for that development.

ACKNOWLEDGMENTS

S. Vakhrushev, A. Levanyuk, and D. Chernyshov are acknowledged for useful discussions. S. Udovenko is acknowledged for his help in setting up x-ray-scattering experiment using the SuperNova diffractometer. R.G.B., I.B., D.A., and G.L. acknowledge the support of Russian Science Foundation (Grant No. 17-72-20083). The optical and dielectric characterization of the crystal has been performed by K. Roleder and J. Piecha under the support of the National Science Centre, Poland, Project No. 2016/21/B/ST3/02242.

APPENDIX A: DETERMINATION OF $\xi_0(T)$ DEPENDENCE

Temperature dependence of the modulation wave-vector component ξ_0 has been characterized independently in the two measurement cycles. The first cycle, diffraction at the ID28 side station, has been carried out at temperatures from 468 K down to 453 K with $\Delta T = 1$ K and an additional point at $T = 423$ K, which corresponds to the bottom of the stability range of the IC phase. The corresponding points are shown by circles in Fig. 6. The smooth dependence shown by a solid line, which is also shown in Fig. 2(d), has been constructed in a way to provide the best approximation to the ID28 points. The second cycle of measurements has been performed using a SuperNova laboratory diffractometer and has been intended to cover the gap in the ID28 data set. The results are shown by triangles. The trend is largely similar, but one notes two quantitative differences. On the one hand, the transition temperatures are different (by about 13 K) for synchrotron and laboratory measurements. On the other hand, the level at which ξ_0 tends to saturate at low temperatures appears slightly lower (by about 0.0005 r.l.u.) for laboratory measurements. Presently, we do not have a reliably verified explanation of these differences.

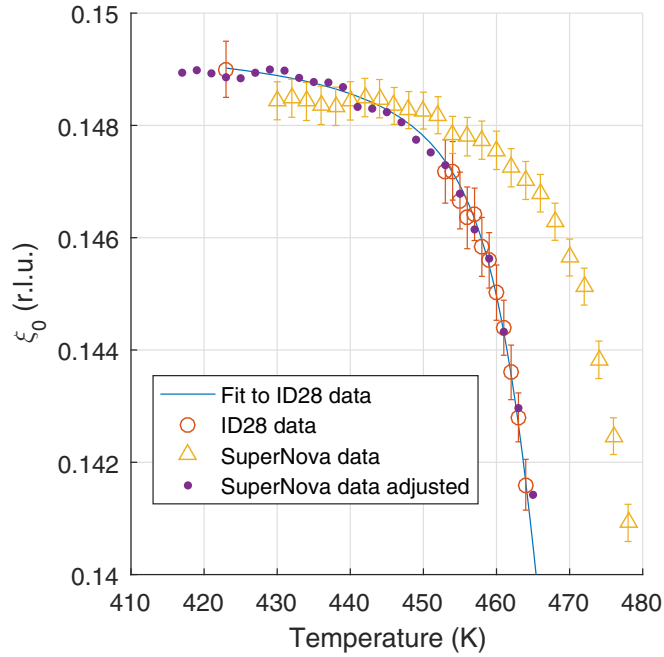

FIG. 6. IC wave-vector component ξ_0 as a function of temperature, as determined in two independent measurement cycles. Circles: data points obtained in the synchrotron experiment at ID28 side station, in the cooling run. Solid line: smooth approximation built on those data points. Triangles: data points obtained in the experiment using SuperNova laboratory diffractometer, in the cooling run. Dots: those points shifted by 13 K in temperature and by 0.0005 r.l.u. in ξ_0.

As to the temperature of the transition between the cubic and $A2$ (IC) phases, its value has been reported previously with the relatively wide spread of about 20 K: from about 468 K [18] to 488 K [12]. The difference in transition temperatures registered by us does not exceed this spread. As a possible source of the difference we can suggest different rates of excess heating due to x-ray absorption [54] in synchrotron and laboratory experiments. Also, the effect could be due to the different mechanical clamping conditions: in the synchrotron experiment the sample was a free-standing needle, while in the laboratory experiment the illuminated area of the sample has been partially covered by the high-temperature glue. Apart

from the above-mentioned differences, the temperature trends of ξ_0 are consistent with each other. Dots show the laboratory data shifted to lower temperatures by 13 K and towards higher ξ_0 by 0.0005. With these adjustments the synchrotron and laboratory dependencies coincide nearly perfectly.

APPENDIX B: WIDTH OF THE *R*-POINT CENTRAL PEAK IN THE WAVE-VECTOR SPACE

The central peak at the *R* point appears rather narrow in the wave-vector space. The nearest points, for which we have recorded IXS spectra (due to the use of multianalyzer setup) are $(1.5, 2.5, 0.5) \pm (0.06, 0.06, 0.01)$. They are away from the *R* point by about 0.085 r.l.u. in the direction ∼[110]. The spectra at these points do not contain a central peak component, indicating that its width in the wave-vector space should be less than 0.085 r.l.u. (≈ 0.125 Å^{-1}). Also we have checked whether the central peak is present along the *R*-*M* line, for which in a similar crystal, $PbZrO_3$, there is an increased intensity of diffuse scattering associated with disordered oxygen tilts [55]. There is no central peak at the middle of this line, at $(1.25, 2.5, 0.5)$. Our results indicate that the central peak does not extend far from the *R* point, but are of lower precision in the wave-vector space than is required for quantitative assessment of the relevant mode dispersion.

[1] T. Janssen and A. Janner, Incommensurability in crystals, Adv. Phys. **36**, 519 (1987).

[2] R. Blinc and A. Levanyk, *Incommensurate Phases in Dielectrics* (North-Holland, Amsterdam, 1986).

[3] R. Caracas and X. Gonze, First-principle study of materials involved in incommensurate transitions, Z. Kristallogr. **220**, 511 (2005).

[4] I. A. Kornev and L. Bellaiche, Planar Defects and Incommensurate Phases in Highly Ordered Perovskite Solid Solutions, Phys. Rev. Lett. **89**, 115502 (2002).

[5] K. Patel, S. Prosandeev, Y. Yang, B. Xu, J. Íñiguez, and L. Bellaiche, Atomistic mechanism leading to complex antiferroelectric and incommensurate perovskites, Phys. Rev. B **94**, 054107 (2016).

[6] R. G. Burkovsky, Dipole-dipole interactions and incommensurate order in perovskite structures, Phys. Rev. B **97**, 184109 (2018).

[7] M. Iizumi, J. Axe, G. Shirane, and K. Shimaoka, Structural phase transformation in K_2SeO_4, Phys. Rev. B **15**, 4392 (1977).

[8] R. Blinc, *Soft Modes in Ferroelectrics and Antiferroelectrics* (North-Holland, Amsterdam, 1974).

[9] Y. Yamada and T. Yamada, Inter-dipolar interaction in $NaNO_2$, J. Phys. Soc. Jpn. **21**, 2167 (1966).

[10] A. D. Bruce and R. A. Cowley, *Structural Phase Transitions* (Taylor and Francis, London, 1981).

[11] A. Cano and A. P. Levanyuk, Defects as a cause of continuity of normal-incommensurate phase transitions, Phys. Rev. B **62**, 12014 (2000).

[12] G. Shirane and R. Pepinsky, Phase Transitions in Antiferroelectric $PbHfO_3$, Phys. Rev. **91**, 812 (1953).

[13] P. Dernier and J. Remeika, Synthesis and symmetry transformation in the perovskite compounds $PbHfO_3$ and $CdHfO_3$, Mater. Res. Bull. **10**, 187 (1975).

[14] N. Leontyev, R. Kolesova, V. Eremkin, O. Fesenko, and V. Smotrakov, Space group of high-temperature lead hafnate orthorhombic phase, Kristallografiya 29, 395 (1984).

[15] H. Fujishita and Y. Ishikawa, Temperature dependence of order parameters in the antiferroelectric phases of perovskite $PbHfO_3$, Ferroelectrics **269**, 135 (2002).

[16] M. Kupriyanov, E. Petrovich, E. Dutova, and Y. V. Kabirov, Sequence of phase transitions in $PbHfO_3$, Crystallogr. Rep. **57**, 205 (2012).

[17] A. Bussmann-Holder, T. H. Kim, B. W. Lee, J.-H. Ko, A. Majchrowski, A. Soszyński, and K. Roleder, Phase transitions and interrelated instabilities in $PbHfO_3$ single crystals, J. Phys.: Condens. Matter **27**, 105901 (2015).

[18] S. Huband, A. Glazer, K. Roleder, A. Majchrowski, and P. Thomas, Crystallographic and optical study of $PbHfO_3$ crystals, J. Appl. Crystallogr. **50**, 378 (2017).

[19] H. Fujishita, K. Kato, E. Nishibori, M. Takata, M. Sakata, and S. Katano, Structural modulations in the intermediate phase of antiferroelectric $PbHfO_3$, J. Phys. Soc. Jpn. **87**, 124603 (2018).

[20] J. Holakovsky, A new type of the ferroelectric phase transition, Phys. Status Solidi B **56**, 615 (1973).

[21] V. Dvořák, Improper ferroelectrics, Ferroelectrics **7**, 1 (1974).

[22] M. Bonin, A. Fuith, K. J. Schenk, and P. Tolédano, Ferroelastic transition triggered by an ordering mechanism in $[(CH_3)_4N]SCN$, Phys. Rev. B **59**, 14246 (1999).

[23] I. A. Kornev and L. Bellaiche, Nature of the ferroelectric phase transition in multiferroic $BiFeO_3$ from first principles, Phys. Rev. B **79**, 100105(R) (2009).

[24] A. Mercy, J. Bieder, J. Íñiguez, and P. Ghosez, Structurally triggered metal-insulator transition in rare-earth nickelates, Nat. Commun. **8**, 1677 (2017).

[25] K. M. Rabe, *Functional Metal Oxides: New Science and Novel Applications* (Wiley-VCH, Weinheim, 2013), pp. 221–244.

[26] A. Girard, T. Nguyen-Thanh, S. Souliou, M. Stekiel, W. Morgenroth, L. Paolasini, A. Minelli, D. Gambetti, B. Winkler, and A. Bosak, A new diffractometer for diffuse scattering studies on the ID28 beamline at the ESRF, J. Synchrotron Radiat. **26**, 272 (2019).

[27] B. Dorner, *Coherent Inelastic Neutron Scattering in Lattice Dynamics* (Springer-Verlag, Berlin, 1982).

[28] P. Bak, Commensurate phases, incommensurate phases and the devil's staircase, Rep. Prog. Phys. **45**, 587 (1982).

[29] R. Burkovsky, I. Bronwald, D. Andronikova, B. Wehinger, M. Krisch, J. Jacobs, D. Gambetti, K. Roleder, A. Majchrowski, A. Filimonov *et al.*, Critical scattering and incommensurate phase transition in antiferroelectric $PbZrO_3$ under pressure, Sci. Rep. **7**, 41512 (2017).

[30] H. Terauchi, H. Takenaka, and K. Shimaoka, Stuctural phase transition in K_2SeO_4, J. Phys. Soc. Jpn. **39**, 435 (1975).

[31] C. J. de Pater and R. B. Helmholdt, Incommensurate structural phase transformation in Na_2CO_3, Phys. Rev. B **19**, 5735 (1979).

[32] In our fit the structure factor has been assumed to vary linearly with scattering vector to account for the observed asymmetry of the profiles.

[33] G. Samara, Pressure and temperature dependence of the dielectric properties and phase transitions of the antiferroelectric perovskites: $PbZrO_3$ and $PbHfO_3$, Phys. Rev. B **1**, 3777 (1970).

[34] D. Andronikova, Y. Bronwald, R. G. Burkovsky, D. Chernyshev, A. Filimonov, B. Nacke, Z. G. Ye, and S. Vakhrushev, Critical X-ray scattering in mixed piezoelectric material $PbZr_{0.6}Ti_{0.4}O_3$, Solid State Phenom. **245**, 211 (2016).

[35] The Curie constant for $PbHfO_3$ is 1.65×10^5 K [33], while for $PbZr_{0.6}Ti_{0.4}O_3$ it can be estimated as an average between the ones of $PbZrO_3$ (1.6×10^5 K [33]) and $PbTiO_3$ (1.1×10^5 K [56]).

[36] P. V. Yudin, R. Ahluwalia, and A. K. Tagantsev, Upper bounds for flexoelectric coefficients in ferroelectrics, Appl. Phys. Lett. **104**, 082913 (2014).

[37] R. Cowley, Lattice dynamics and phase transitions of strontium titanate, Phys. Rev. **134**, A981 (1964).

[38] R. G. Burkovsky, D. Andronikova, Y. Bronwald, M. Krisch, K. Roleder, A. Majchrowski, A. V. Filimonov, A. I. Rudskoy, and S. B. Vakhrushev, Lattice dynamics in the paraelectric phase of $PbHfO_3$ studied by inelastic x-ray scattering, J. Phys.: Condens. Matter **27**, 335901 (2015).

[39] P. Ghosez, E. Cockayne, U. V. Waghmare, and K. M. Rabe, Lattice dynamics of $BaTiO_3$, $PbTiO_3$, and $PbZrO_3$: A comparative first-principles study, Phys. Rev. B **60**, 836 (1999).

[40] A. Glazer, Simple ways of determining perovskite structures, Acta Crystallogr. Sect. A **31**, 756 (1975).

[41] The signal due to Γ_{15} phonons is strong in all Brillouin zones. It is therefore virtually impossible to separate AFD signal and Γ_{15} signal in the IXS experiment by choosing the appropriate zone. Inelastic neutron scattering, with which this could be possible, is inapplicable for this crystal because of small sizes of the available single-crystal samples.

[42] R. A. Cowley and S. M. Shapiro, Structural phase transitions, J. Phys. Soc. Jpn. **75**, 111001 (2006).

[43] T. Riste, E. Samuelsen, K. Otnes, and J. Feder, Critical behavior of $SrTiO_3$ near the 105 K phase transition, Solid State Commun. **9**, 1455 (1971).

[44] S. Shapiro, J. Axe, G. Shirane, and T. Riste, Critical neutron scattering in $SrTiO_3$ and $KMnF_3$, Phys. Rev. B **6**, 4332 (1972).

[45] J. Töpler, B. Alefeld, and A. Kollmar, Investigation of the central component of $SrTiO_3$ by neutron scattering with eV resolution, Phys. Lett. A **51**, 297 (1975).

[46] C. Darlington, W. Fitzgerald, and D. O'connor, On the energy width of the central mode in the critical scattering of X-rays by $SrTiO_3$, Phys. Lett. A **54**, 35 (1975).

[47] A. Tagantsev, K. Vaideeswaran, S. Vakhrushev, A. Filimonov, R. Burkovsky, A. Shaganov, D. Andronikova, A. Rudskoy, A. Baron, H. Uchiyama *et al.*, The origin of antiferroelectricity in $PbZrO_3$, Nat. Commun. **4**, 2229 (2013).

[48] W. Zhong and D. Vanderbilt, Competing Structural Instabilities in Cubic Perovskites, Phys. Rev. Lett. **74**, 2587 (1995).

[49] L. Bellaiche and J. Iniguez, Universal collaborative couplings between oxygen-octahedral rotations and antiferroelectric distortions in perovskites, Phys. Rev. B **88**, 014104 (2013).

[50] P. Goudochnikov and A. J. Bell, Correlations between transition temperature, tolerance factor and cohesive energy in 2+: 4+ perovskites, J. Phys.: Condens. Matter **19**, 176201 (2007).

[51] J. Hlinka, T. Ostapchuk, E. Buixaderas, C. Kadlec, P. Kuzel, I. Gregora, J. Kroupa, M. Savinov, A. Klic, J. Drahokoupil *et al.*, Multiple Soft-Mode Vibrations of Lead Zirconate, Phys. Rev. Lett. **112**, 197601 (2014).

[52] J. Íñiguez, M. Stengel, S. Prosandeev, and L. Bellaiche, First-principles study of the multimode antiferroelectric transition in $PbZrO_3$, Phys. Rev. B **90**, 220103(R) (2014).

[53] R. G. Burkovsky, A. K. Tagantsev, K. Vaideeswaran, N. Setter, S. B. Vakhrushev, A. V. Filimonov, A. Shaganov, D. Andronikova, A. I. Rudskoy, A. Q. R. Baron *et al.*, Lattice dynamics and antiferroelectricity in $PbZrO_3$ tested by x-ray and Brillouin light scattering, Phys. Rev. B **90**, 144301 (2014).

[54] H. Wallander and J. Wallentin, Simulated sample heating from a nanofocused x-ray beam, J. Synchrotron Radiat. **24**, 925 (2017).

[55] M. Paściak, T. Welberry, A. Heerdegen, V. Laguta, T. Ostapchuk, S. Leoni, and J. Hlinka, Atomistic modeling of diffuse scattering in cubic $PbZrO_3$, Phase Transit. **88**, 273 (2015).

[56] V. Bhide, K. Deshmukh, and M. Hegde, Ferroelectric properties of $PbTiO_3$, Physica **28**, 871 (1962).